

Cooper Union Mars Ascent Vehicle

Team Members (all undergraduates)

Alexander Seligson, *Mechanical Engineer*

Harris Paspuleti, *Mechanical Engineer*

Andrew Huh, *Mechanical Engineer*

Hannah Quirk. *Mechanical Engineer*

Faculty Adviser

Professor Sven Haverkamp

Cooper Union

March 4th, 2021

1 Quad Chart



Cooper Union Mars Ascent Vehicle



<p>Objectives & Technical Approach:</p> <ul style="list-style-type: none">• Major project objectives<ul style="list-style-type: none">• Minimize cost with optimized trajectory and materials• Minimize weight using novel TPS and Propulsion• Description of technical approach<ul style="list-style-type: none">• Hybrid propulsion system with in-situ propellant production• Two stages	<p>Image:</p>
<p>Team & Management Approach:</p> <ul style="list-style-type: none">• Team: Alexander Seligson, Andrew Huh, Hannah Quirk, Harris Pasqualeti• Advisor: Prof. Sven Haverkamp• Management approach:<ul style="list-style-type: none">• Alexander Seligson—Thermal, Trajectory, Electrical Power• Andrew Huh—Structures, weights, CAD• Hannah Quirk—Propulsion• Harris Pasqualeti—Cost Analysis, Egress/Ingress	<p>Schedule:</p> <p>List of major milestones for project lifecycle</p> <ul style="list-style-type: none">• 2025: phase A: Concept Development• 2026: phase B: Preliminary Design and Fabrication• 2029: phase C: Final Design and Fabrication• 2031: phase D: System Assembly and Integration• 2033: phase E: Launch Operation <p>Cost:</p> <ul style="list-style-type: none">• Total proposed budget: ~ \$9.6 Billion

Contents

1 Quad Chart	ii
2 System Overview	1
2.1 Cost Estimate	1
2.2 Product Development Timeline	2
3 Trajectory	2
4 Propulsion	4
5 Thermal Protection System	6
5.1 Atmospheric Heating	6
5.2 Rocket Motor Thermal Protection	8
6 Structures	8
6.1 Exterior and Interior Frames	8
6.2 Avionics	9
6.3 Power	9
7 Future Work	9
A Appendix A: Propulsion System Operation Parameters	10
B Appendix B: Propulsion System Equations	11
C Appendix C: Thermal System Equations	12
C.1 1D Thermal Simulation Equations	12

2 System Overview

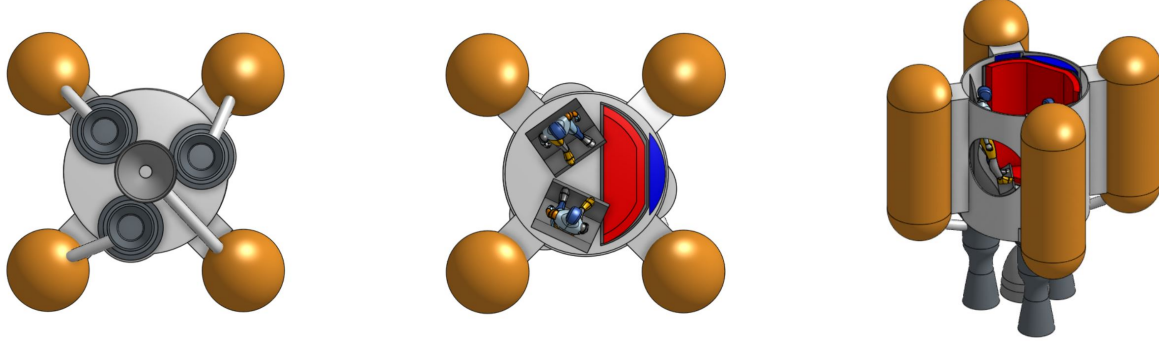


Figure 1: Bottom, Top, and Isometric View of the MAV

The Mars Ascent Vehicle (MAV) design was broken down into the propulsion system, the thermal protection system, and the structures system.

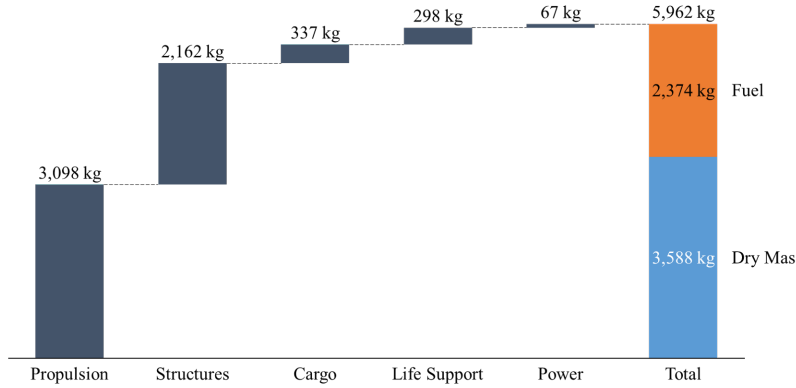


Figure 2: Mass Overview

Each system produced a minimum and maximum mass estimate. The average mass for each system is displayed in Figure 2 and is significantly lower than the RASC-AL dry and wet mass requirements. It should be noted that the 121 kg thermal mass was included in structures mass. The maximum possible dry mass is 3737 kg due to the possible differences in the manufactured thickness of structural components.

The cargo and life support estimates were determined from the four-person MAV report from NASA that had per person per day requirements listed [1].

2.1 Cost Estimate

The estimated cost was calculated using techniques described by Dr. Arney and Dr. Wilhite [2]. Using a series of Cost Estimating Relationships (CERs) that require basic information from the system sizing tools, a budget was developed for the proposed MAV. This initial cost estimate provides evidence that the

proposed MAV is financially feasible in regards to the allocated budget for the project. A summation of all the Design, Development, Testing, and Evaluation (DDT&E) costs and flight unit costs for every MAV subsystem resulted in a total estimated budget of \$9.6 billion for the MAV. Figure 3, below, shows the MAV subsystem cost breakdowns.

Subsystem:	Subsystem DDT&E Cost (\$M)	Flight Unit Cost (\$M)	Total Subsystem Cost (\$M)
Crew Capsule	1872.40	272.89	2145.28
Ascent Stage (Storable)	2060.82	222.56	2283.38
In-space Habitat	2750.07	228.94	2979.01
Propulsive Stage	1111.28	85.39	1196.67
Propellant Depot	958.90	110.42	1069.32
		Total Cost (\$M)	9673.67

Figure 3: MAV subsystem breakdown cost estimates: DDT&E costs, Flight unit costs, and Total costs

The techniques described in the Rapid Cost Estimation paper [2] account for costs being distributed over multiple years through the use of a beta distribution curve. The cost estimation accounts for standard practices at NASA and operates on an 60:40 spread in which 60% of the cost is spent over the first half of the project and the remaining 40% of the cost is spent over the second half of the project. NASA uses this standard for technically challenging designs and manned systems in which more money must be committed early in the development period.

2.2 Product Development Timeline

- 2025: Phase A: Concept Development
- 2026: Phase B: Preliminary Design and Fabrication
- 2029: Phase C: Final Design and Fabrication
- 2031: Phase D: System Assembly and Integration
- 2033: Phase E: Launch Operation

3 Trajectory

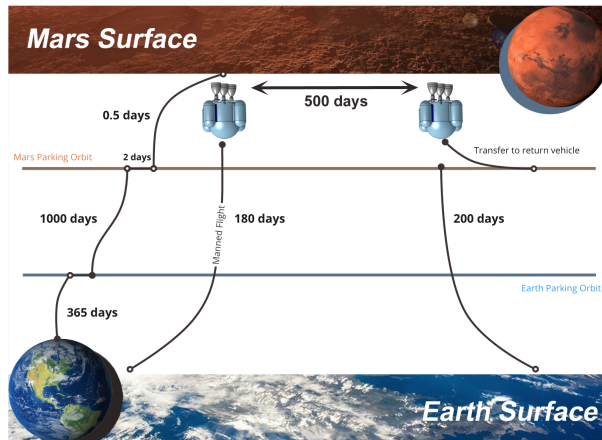


Figure 4: Mission Timeline

The trajectory of the MAV to Mars was researched for three main reasons. First, to find a suitable parking orbit for the return vehicle—information that drives many decisions for the MAV’s design. Second, to determine the MAV entry velocity, and third, to plan out the mission timeline. The trajectories were analyzed by looking at the change in velocity (ΔV), the number of launch opportunities, the travel time, the associated risk, and the vehicle’s entry velocity.

The MAV first travels without a crew from Earth to Mars. This occurs four years prior to the manned flight. The first flight will use a minimum energy Hohmann transfer orbit to reach Mars. Ion thrusters will propel the MAV because of their cost and mass savings. While this increases transit time, this is not a concern because the MAV is unmanned during this stage [1].

For the manned flight, Earth to Mars trajectories with travel times varying from 100 days to approximately 550 days were analyzed. Since Mars and Earth are in a 15-year periodic cycle with each other, Earth to Mars trajectories plotted over a 15-year span can be extrapolated to apply for any time after that. A weighted decision matrix, shown in Table 1, was created in order to find the most suitable option for the mission. It was found that the 180-day conjunction class trajectory offered the best balance among the selected criteria.

			Paths						
			Opposition Class	Free Return	Conjunction Class				
			Dash/Venus swing	2 year cycle	3 year cycle	Hohman transfer	120 day	180 day	270 day
Criteria	ΔV	5	2	3	4.5	5	3	3.75	4.25
	Time of Flight	4	5	2.5	2	1	4.75	4.5	3.5
	Time on Mars	4	2	4	4	4	5	4.75	4
	Entry Speed	3	1	2.5	3.5	4	2	3	4
	Structural mass	3	3.5	3	2.75	2.75	3.5	3.25	3
	Radiation Exposure	3	1	3.25	3	2.75	5	4	3.75
	Readiness level	2	4	2	4	4	2.75	4	4
	Abort option	1	1	5	4	3	1	1	1
	Sum		63.5	76.25	86.25	84.5	92	94.5	92.5

Table 1: Trajectory Decision Matrix. Table displaying the trajectories considered and their weighted scores.

After the 180 day flight, the rocket will perform an Aerocapture maneuver to enter a 250 km by 33,900 km elliptical orbit [3]. This is commonly called a 1-Sol orbit.

The three main options considered for the Mars to 1-Sol trajectory were a 48-hour, 24-hour, and 12-hour rendezvous. Looking at the ΔV and using the 48-hour trajectory as a baseline, the 24-hour trajectory cut the time of ascent in half while only increasing the ΔV by 3 m/s [1]. The 12-hour trajectory took a quarter of the time but required an extra 170 m/s ΔV . As the time of flight decreased, the number of possible launch opportunities also shrunk [1]. A 48-hour trajectory has multiple launch opportunities per day while a 24-hour trajectory is only able to launch a few times a month. The 12-hour trajectory was even more infrequent [1]. The 24-hour trajectory was chosen because it has a relatively small ΔV penalty while reducing the overall time of flight by half. The smaller quantity of launch windows was deemed a suitable risk because there would still be several opportunities to launch per month.

4 Propulsion

The propulsion system for the Mars Ascent Vehicle provides the thrust necessary to propel the MAV from the surface of Mars to a 1-Sol orbit. It was determined that the optimal ΔV for this mission was 5274 m/s, so the fuel requirements were shared around achieving that ΔV . The proposed MAV will use a two-stage hybrid propulsion system with a paraffin-based wax as the fuel and liquid oxygen oxidizer collected using an in-situ propulsion system. The system will use three 125kN engines for the first stage, and one for the second stage.

A two-stage system was selected for its fuel efficiency and failure modes. With a two-stage system, the tanks from the first stage can be ejected upon completion. This means that the second stage can continue propulsion with less mass. A two-stage system also allows for higher safety margins against failure modes, which is desirable. Calculations for mass differences between a single stage and a two stage system for a four-person MAV were obtained from Polsgrove et al. [1]. A single stage system would require an excess ΔV of 275 m/s to reach just a 500km final orbit. The MAV would have to rendezvous with a taxi vehicle to carry the crew from the 500km orbit to the return vehicle in the 1-sol orbit. It was decided that this added complexity and cost outweighs the mass benefits of the single stage to orbit system. The results from Polsgrove et al., run in NASA POST, are shown in Figure 5. There are only 6% mass savings between the single stage to orbit and two stage to 1-Sol orbit systems.

Table 4. MAV Vehicle Trades and Assumptions. Vehicle options and mass assumptions that are used in the mass sensitivities to thrust and launch latitude.

	Stages to Orbit	Orbit	Payload	Propellant	Isp	Stage PMF	
						1 st Stage	2 nd Stage
Option 1	SSTO	500 km Circular	3,919 kg	NTO/MMH	335 s	0.86	--
Option 2A	TSTO, 2 Engine 1 st Stage	1 sol	4,178 kg	LOX/LCH ₄	360 s	0.83	0.73
Option 2B	TSTO, 3 Engine 1 st Stage	1 sol	4,178 kg	LOX/LCH ₄	360 s	0.83	0.73
Option 3A	TSTO, 2 Engine 1 st Stage	5 sol	4,326 kg	LOX/LCH ₄	360 s	0.83	0.73
Option 3B	TSTO, 3 Engine 1 st Stage	5 sol	4,326 kg	LOX/LCH ₄	360 s	0.83	0.73

Figure 5: Comparison of single stage to orbit and two stage to orbit designs [1]

A hybrid propulsion system was selected for this mission for its higher specific impulse, large range of operating temperatures, and safety. The paraffin-based wax does not require temperature control, which eliminates most of the cryogenic liquid and cooling systems necessary for conventional propulsion systems. This greatly reduces lift-off mass from Earth. The paraffin wax will be brought from Earth, while the liquid oxygen (LOX) will be produced on Mars using an in-situ propellant production system (ISPP) originally proposed by Boiron et al. [4].

To produce the LOX, CO_2 collected on Mars will be decomposed into O_2 using a Zirconia membrane solid oxide electrolysis system. This decomposition happens in two steps. First, the CO_2 is thermally and catalytically decomposed into CO and O_2 close to the Zirconia membrane. The Zirconia membrane has a voltage passed through it so it can then capture and extract the oxygen ions and recombine those ions into dioxygen.

The three 125 kN engines were selected for their commercial availability and thrust capability. The engine thrust vs. liftoff mass was based on calculations done for a LOX/LCH_4 propulsion system. From Figure 6,

it can be seen that the optimum engine thrust per liftoff mass is from the three-engine system at 125 kN of thrust per engine. The two-engine case causes a higher overall liftoff mass, which is undesirable.

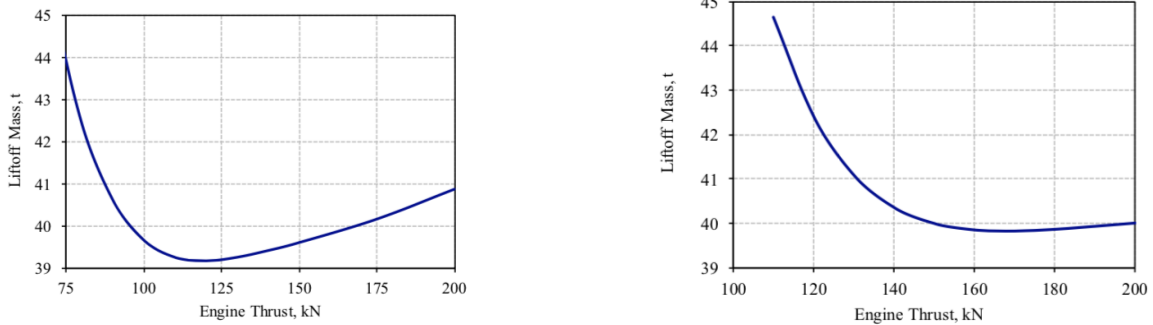


Figure 6: Comparison of MAV liftoff mass vs. engine thrust for three and two engine MAV case [1]

For the ISPP system to operate, it requires dust filtering, compression, heating, and cryocooling subsystems. The parameters for each of these components are in Appendix A. Masses for the ISPP system were found by sizing the Zirconia cell based on the total amount of oxidizer needed for the system, and the capabilities of the Zirconia membrane to produce that oxidizer. The total amount of oxidizer needed for the mission was found to be 2,500 kg. For a 500-day mission duration, that means the system must produce 5.0 kg of oxidizer per 24.4hr sol. The resulting requirements of the Zirconia cell are shown below in Table 2. These parameters from the sizing of the Zirconia cell were then used to create mass and power budgets for the system, shown below in Tables 3 and 4. A generous 20% margin was applied following methods referenced in Chandler et al. [5].

Table 2: Zirconia cell sizing

	Units	
Total current	637	A
Cell power	1082	W
Cell area	1591	cm ²
# of 10cm wafers	22	
Wafer area	1521	cm ²
ZrO ₂ system mass	20	kg
Stack heat loss	220	W
CO ₂ extraction rate	635	g/hr
Sorption comp. power	217	W
Sorption comp. mass	22	kg

Table 3: Mass budget

	kg
ZrO ₂ system	19.8
Sorption comp.	21.7
Cryocooler	20.2
Dust filter	1.2
Heat exchanger	0.8
Other	39.0
ASRG	266.8
Total	369.5

Table 4: Power budget

	W
ZrO ₂	1301.7
Sorption	217.5
Cryocooler	268.3
Total	1787.4

To determine whether the ISPP system would lead to overall mass savings for the MAV, it was compared to the same proposed MAV structure where both the oxidizer and the fuel were brought from launch on Earth. Comparing the mass of the non-ISPP system to the ISPP system, the In-Situ system has a 48.9% in-situ gain as shown in Table 5. In-situ gain compares the savings between the lift-off mass and the hybrid ISPP system mass while accounting for the additional mass of the ISPP unit itself. The Earth launch mass for the ISPP system is approximately 2,700 kg lighter than the non-ISPP system. The calculations for the ISPP unit mass, the system brought mass, and the in-situ gain can be found in Appendix B.

System	Mass (kg)
Lift-off mass (non-ISPP)	6999
Rocket brought mass	4476
ISPP unit mass	370
System brought mass (ISPP)	4846
In-Situ Gain	48.62%

Table 5: Mass comparison of hybrid-ISPP system vs. traditional hybrid system

5 Thermal Protection System

The goal of the Thermal Protection System (TPS) is to protect the MAV from excess heat. The two main sources of heat are from the hot gas plumes of the rocket engine and the atmospheric compression upon landing and takeoff.

5.1 Atmospheric Heating

To protect the main structure from the heat generated during takeoff, 0.5 inches of Advanced Flexible Reusable Surface Insulation (AFRSI) blanket with a Protective Ceramic Coating (PCC) will be adhered to the exterior of the MAV. This material was selected for its light weight, affordability, and maximum operational temperature. Table 6 shows the considered materials, costs and max effective temperature.

material	Max temp (K)	Material Cost (\$1000/m ²)
Carbon fiber CMC (C/SiC)	1922	161.46
Advanced C-C (ACC)b	1866	129.17
Shuttle coated C-C (RCC)	1755	129.17
AETB-8/TUFI	1700	8.61
LI-900/RCG	1533	12.51
TABI (PCC coating)	1366	11.09
AFRSI-HT (PCC coating)	1478	5.38
AFRSI (C-9 coating)	922	3.55
PBI felt (VHT coating)	810	2.55
FRSI (DC92 coating)	644	1.72
Nickel super-alloy tile	1311	47.90
Nickel super-alloy sheet	1255	47.90
Titanium multiwall	866	64.96

Table 6: TPS Materials Considered. [6]

A simple 1-D heat transfer model was developed to approximate the compressive heating of the MAV to ensure it was within operational temperatures. To do this, several key assumptions were made. These assumptions include a vertical launch trajectory, a thrust launch weight ratio of 2, negligible drag, and a propellant exit velocity of 3000 m/s. The elapsed time, MAV mass, altitude, and speed were then iteratively calculated. Using an atmospheric lapse rate [7] and knowing the MAV velocity, the mach number was calculated. Due to the MAV's blunt shape, a bow shock wave model was used to find the stagnation temperature at the tip of the rocket. Figure 7 displays the convective heat transfer coefficient and stagnation temperature as a function of altitude. The equations used for the heat transfer coefficient calculation are included in Appendix C.

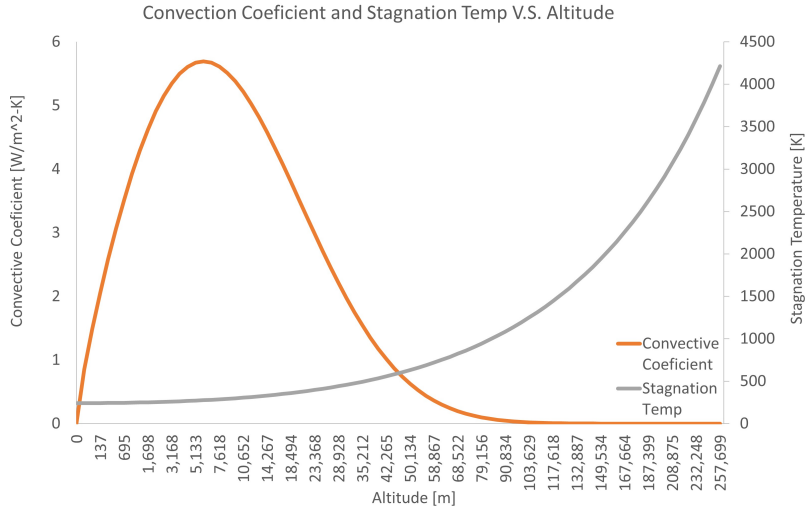


Figure 7: Stagnation temperature at the tip of the MAV for a given altitude

It should be noted that the stagnation temperatures are much higher than 1500 K. This is not an issue because the system only reaches such high temperatures in the upper atmosphere, where the convective heat transfer coefficient is very close to zero. This means little to no heat transfer will occur. At 100,000 m the stagnation temperature is about 1200 K and the convective heat transfer coefficient approaches 0, so a 1000 K estimate for the heat shield temperature is reasonable and is in line with Lobbia et al. [8].

A simplified 1-D heat transfer circuit model was created, as shown in Figure 8. The temperature with and without the AFRSI TPS are in Figure 9. Without the TPS the frame reaches 475 K, the temperature where the aluminum is at half its original yield strength, in 11.5 min while with the TPS the frame doesn't reach that temperature during the ascent.

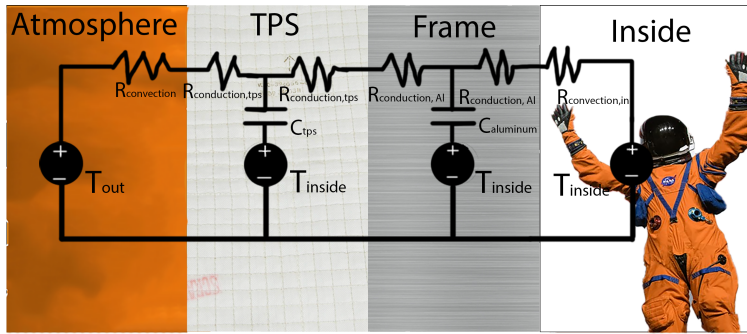


Figure 8: 1-D Thermal circuit used for heat transfer model

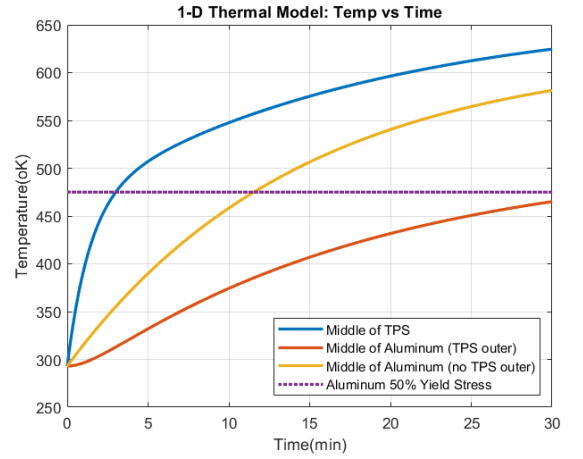


Figure 9: Temperature of Aluminum With and Without TPS

5.2 Rocket Motor Thermal Protection

Sella et al. [9] outlines a method for protecting the structure of a rocket from rocket plumes emitted by the MAV engine. An ablative phenolic canvas is placed between the fuel grain and the combustion chamber's inner wall. This protects the chamber from high temperatures and pressures of the motor. Phenolic canvas was chosen for its poor thermal conductivity, ablation at a slow rate of between $0.02 - 0.09 \text{ mm/s}$, and its reliability as shown through testing for small scale models.

6 Structures

The MAV structure is comprised of an exterior vehicle frame and permanently fixed interior components including control panels, seats, and environmental control systems. The complete vehicle is divided into three main parts:

- The cabin that holds all crew and mission necessities and a living space
- Fuel tanks for both solid and liquid fuel
- The engines that are part of the propulsive system.

The vehicle cabin (excluding the fuel tanks) equals approximately 13 cubic meters, including

- The crew space
- The equipment section
- Avionics and other electronics.

The propulsion system is placed directly under the cabin area. Three fuel tanks supply the fuel for the three first stage engines, and explosive bolts are used to discard the first stage tanks. The other tank connects to the second stage engine.

6.1 Exterior and Interior Frames

The exterior system includes the frame, tank, and other structural components. The inner frame is manufactured using aluminum 7075, and is connected to a layer of AFRSI as mentioned in the thermal protection system section. The mass for the frame is estimated between 440 kg and 488 kg. This estimation is calculated based on material density and production thicknesses. While the minimum thickness is just enough for heat protection, the manufacturing constraints and structural analysis can cause an increase in mass.

The tank uses PTFE as its inner frame to withstand pressures from the liquid oxygen fuel and Surface foam Insulator (SOFI) for its thermally protective coating. The mass for the tank is estimated between 676 kg and 831 kg. Similar to the frame, the mass was calculated by using the material density and required volume for the two types of fuel, and the mass estimate disparity occurs due to manufacturing constraints.

The other structural components include sections such as the fuel pump, fuel lines, inner frame components, and material connections. Since the pumps and lines are approximately cylinders, they were calculated using the same method as the the cabin frame with the same material. The mass is estimated between 538 kg and 585 kg. Using a fixed aluminum skin thickness of 5 mm, the frame's mass differences highly depended on the chosen thickness of AFRSI. This totals to an average of 2162.3 kg for the exterior mass.

6.2 Avionics

The mass assessment for avionics is dependent on functional aspects. As a result, the mass estimate was decided to be 407 kg—the same as the four person MAV listed Polsgrove et al. [10]. This value also includes the control panel that is inside the crew compartment.

The avionics of the vehicle is located at the upper hemispherical cap. This area is not only easily accessible for the crew, but also saves cabin space, which is designed to be compact for the necessary cargo.

6.3 Power

Altair [11] [12] and the 4 person MAV concept [10] were used to get a baseline for power requirements. Both of these vehicles provide a conservative estimate for power needs since the estimated power requirements for the 4 person Altair vehicle were driven by the 7 day ‘sortie’ mission where astronauts would be living in the ascent vehicle (requiring significant electrical power) and the 4 person MAV has 2 more people (that drive up electrical requirements for life support). Although both concepts use fuel cells for power at some point, the Altair vehicle uses batteries for to power the ascent phase. Which gives a good baseline for the 2 person MAV.

	Altair[12]	4 person MAV[10]
System Type	Battery	Fuel Cell
Energy requirement [kW-h]	14	10
mass [kg]	67	377

Table 7: Altair and 4 person MAV power system

The highest energy requirement estimate for either the Altair or the 4 person MAV was 14 kW-h. Thus the 2 person MAV concept features a similar 62 kg, 14 kW-h, silver-zinc (Ag-Zn) battery. This battery was chosen because of its high energy density and its previous track record in space. Although in the past, the Ag-Zn battery has had some issues after several recharging cycles, this should not be a problem since few recharging cycles will be required during the mission.

7 Future Work

These are tasks that are still being worked on:

- Calculate Exact Nozzle Dimension’s
- Scope out Exact Power Usage
- Optimize Stage 1 and Stage 2 Fuel Ratio
- Obtain Better Mass Ranges with Factors of Safety Considered
- Incorporate Different Materials in Mass and Cost Estimate of Frame
- Perform Load Analysis on Frame
- Analyze Thermals for MAV EDL

A Appendix A: Propulsion System Operation Parameters

RPS system parameters			
Power production	6.7 We/kg of specific power		
Zirconia cell parameters			
O_2 production rate	0.325	g/hr	per 1A
Current density	0.4	A/cm^2	
Cell voltage	1.7	V	
CO_2 conversion efficiency	90%		
System specific mass	5.4	kg	per 440cm of wafer area
Heat loss	10	W	per wafer
Dust filtering			
Filter capabilities	0.6	kg	per 2.5kg O_2 per 24.4hr day
Compression			
Compressor mass	6	kg	
CO_2 production	175	h/hr	CO_2 for 60W of power
Heating			
Heater mass	0.4	kg	per 2.5kg of O_2 per 24.4hr day
Cryocooler			
Cryocooler mass	10	kg	per 2.5kg O_2 per 24.4hr day
Cryocooler power	70	W	per 2.5kg O_2 per 24.4hr day

B Appendix B: Propulsion System Equations

Knowing the ΔV required for the first and second stage, the payload mass m_{PL} as well as the specific impulse I_{sp} delivered by the system at the set O/F ratio, the required propellant for the first and second stage were found by rearranging the equation and solving for m_o , where m_o is the empty mass, propellant mass, and payload mass.

$$\frac{\Delta M}{m_o} = 1 - \exp - \frac{m_{PL}}{m_o - m_{PL}}$$

Then, λ , the payload fraction was found

$$\lambda = \frac{m_{PL}}{m_E + m_p}$$

and set equal to

$$\lambda = \frac{1 - \epsilon \exp \frac{\Delta V}{ng_o I_{sp}}}{\exp \frac{\Delta V}{ng_o I_{sp}}}$$

where n is the number of stages, and ϵ is the structural efficiency set at 0.18 following methods outlined in Boiron et al. [4]. The payload ratios were found for both stage 1 and stage 2. Then, knowing the amount of propellant required, m_p , the corresponding amounts of fuel and oxidizer were found by comparing the total amount of propellant required to the O/F ratio. The fuel mass, m_f was found by taking

$$m_f = \frac{m_p}{1 + O/F}$$

and the oxidizer mass m_{ox} was found by taking

$$m_{ox} = m_f \cdot O/F$$

The in-situ gain was defined as

$$G_{in-situ} = \frac{O/F}{1 + O/F} (1 - \Gamma)(1 - \epsilon) - \frac{m_{ispp}}{m_{lifttoff}}$$

where Γ is the payload fraction defined for n identical stages

$$\Gamma = \left(\frac{1 - \epsilon \exp \frac{\Delta V}{ng_o I_{sp}}}{(1 - \epsilon) \exp \frac{\Delta V}{ng_o I_{sp}}} \right)^n$$

C Appendix C: Thermal System Equations

Lapse rate of Martian Atmosphere: $P[atm] = \frac{.699e^{(-0.00009*H[m])}}{101.3}$ [7]

The convective heat transfer coefficient was calculated by finding:

The Prandtl number: ($Pr = \frac{\mu*C_p}{\rho*K}$)

The Reynolds number: ($Re = \frac{\rho*V*D}{\mu}$)

The Nusselt number ($Nu = .037 * Re^{0.8}$ assuming $Pr = 0.7$ and $0 < Re < 70000$) and finally using $H = \frac{Nu*K}{D}$ to find the convection coefficient [13]

C.1 1D Thermal Simulation Equations

Using Kirchhoff's current law on the circuit in Figure 8, These thermal equations were found. T2 is the node corresponding to the temperature in the middle of the TPS and T4 is the node corresponding to the temperature in the middle of the Aluminum. (The equations are in the Laplace domain):

$$T_2\left(\frac{1}{R_{conv,out} + \frac{R_{tps}}{2}} + \frac{2}{R_{tps} + R_{Al}} + SC_{tps}\right) - T_4\left(\frac{2}{R_{tps} + R_{Al}}\right) = \frac{\frac{T_{out}}{S}}{R_{conv,out} + \frac{R_{tps}}{2}} + T_{in}C_{tps}$$

$$-T_2\left(\frac{2}{R_{tps} + R_{al}}\right) + T_4\left(\frac{1}{R_{conv,in} + \frac{R_{Al}}{2}} + \frac{2}{R_{tps} + R_{Al}} + SC_{Al}\right) = \frac{\frac{T_{in}}{S}}{R_{conv,in} + \frac{R_{Al}}{2}} + T_{in}C_{AL}$$

The equations were put into $[A][X]=[b]$ matrix form of where

$$[A] = \begin{bmatrix} \left(\frac{1}{R_{conv,out} + \frac{R_{tps}}{2}} + \frac{2}{R_{tps} + R_{Al}} + SC_{tps}\right) & -\left(\frac{2}{R_{tps} + R_{Al}}\right) \\ -\left(\frac{2}{R_{tps} + R_{al}}\right) & \left(\frac{1}{R_{conv,in} + \frac{R_{Al}}{2}} + \frac{2}{R_{tps} + R_{Al}} + SC_{Al}\right) \end{bmatrix}$$

,

$$[X] = \begin{bmatrix} T2 \\ T4 \end{bmatrix}$$

and

$$[B] = \begin{bmatrix} \frac{\frac{T_{out}}{S}}{R_{conv,out} + \frac{R_{tps}}{2}} + T_{in}C_{tps} \\ \frac{\frac{T_{in}}{S}}{R_{conv,in} + \frac{R_{Al}}{2}} + T_{in}C_{AL} \end{bmatrix}$$

the system of equations was solved for X in the Laplace domain and then the time domain step response was taken which resulted in Figure 9,

References

- [1] Polsgrove, Tara, et al. "Mars Ascent Vehicle Design for Human Exploration." *AIAA SPACE 2015 Conference and Exposition, 2015* doi:10.2514/6.2015-4416.
- [2] Arney, Dale., et al. "Rapid Cost Estimation for Space Exploration Systems." *AIAA, 2012*
- [3] Young, Archie C. "Mars Mission Profile Options and Opportunities." *The Space Conference Proceeding, 1988* Sept. 2018 Link
- [4] Boiron, Adrien J., and Brian Cantwell. "Hybrid Rocket Propulsion and In-Situ Propellant Production for Future Mars Missions." *49th AIAA/ASME/SAE/ASEE Joint Propulsion Conference, 2013* doi:10.2514/6.2013-3899.
- [5] Chandler, Ashley J., et al. "Feasibility of a single port Hybrid Propulsion system for a Mars Ascent Vehicle" *Chancellor's Honors Program Projects, 2019* doi:10.1016/j.actaastro.2011.07.004
- [6] D. Rasky, D. J, et (Rasky, Milos, Squire, 2001) al. "Thermal Protection System Materials and Costs for Future Reusable Launch Vehicles." *SPACECRAFT, vol. 38, no. 2* doi:10.2514/2.3686
- [7] Hall, Nancy. "Mars Atmosphere Model - Metric Units." *NASA, NASA, 2015*, www.grc.nasa.gov/www/k-12/airplane/atmosrm.html.
- [8] Lobbia, Marcus, et al. "Mars Ascent Vehicle Concept – Overview and Aeroheating/Thermal Protection System Design." *NASA, 2017* Link
- [9] Sella, Vignesh, et al. "Development of a Nytrox-Paraffin Hybrid Rocket Engine." *AIAA Propulsion and Energy 2020 Forum, 2020* doi:10.2514/6.2020-3729
- [10] Polsgrove, Tara P., et al. "Human Mars Ascent Vehicle Configuration and Performance Sensitivities" *NASA, NASA, 2017*
- [11] Tara P., et al. "Altair Lunar Lander Consumables Management" *AIAA, 2009*
- [12] Miller, Thomas B., "Human Mars Ascent Vehicle Configuration and Performance Sensitivities" *NASA, NASA, 2014*
- [13] Holman, Jack P., "Heat Transfer" *McGraw-Hill, 2008*